Synthesis of Mesoporous Supraparticles on Superamphiphobic Surfaces

Sanghyuk Wooh, Hannah Huesmann, Muhammad Nawaz Tahir, Maxime Paven, Kristina Wichmann, Doris Vollmer, Wolfgang Tremel, Periklis Papadopoulos, and Hans-Jürgen Butt**

Dr. S. Wooh, M. Paven, Dr. D. Vollmer, Prof. H.-J. Butt
Max Planck Institute for Polymer Research, Ackermannweg 10, D-55128, Mainz, Germany
E-mail: butt@mpip-mainz.mpg.de
H. Huesmann, Dr. M. N. Tahir, K. Wichmann, Prof. W. Tremel
Institute of Inorganic Chemistry, University of Mainz, Duesbergweg 10-14, D-55099, Mainz, Germany
Prof. P.Papadopoulos
Physics Department, University of Ioannina, P.O. Box 1186, GR 45110, Greece
E-mail: papadopo@cc.uoi.gr

Mesoporous particles have found numerous applications in science and daily life, such as catalyst[1], biomaterials[2], and as energy producing[3] or storage materials[4]. Mesoporous particles with uniform and large pore volume are synthesized with the aid of templates, such as surfactants in a modified Stöber process,[5, 6] or by self-assembly of nano-objects[7, 8] in solution. Both processes are suitable for large-scale production, but they are energy consuming and produce chemical waste. Moreover, the engineering of size and composition requires additional chemicals for fine-tuning the synthetic variables. It is a relevant task to develop new approaches to overcome shortcomings of the solution-based processes by reducing or completely avoiding any type of solvent, emulsifier or template. Recently, the opal structure formation by evaporation of sessile drops containing nano- or micro-colloids on the superhydrophobic surfaces[9] has been introduced as a possible strategy for the synthesis of supraparticles. However, the strong adhesion between drops and surface restricted the formation of the supraparticles, impeded their separation, and limits the choice of dispersions. Superamphiphobic surfaces extend the water repellent properties of superhydrophobic surfaces to nonpolar liquids.[10, 11]. On such a surface, drops of nearly any liquid have high contact angles (CA > 150˚) and roll-off easily (tilting < 10˚). The synthetic potential of superamphiphobic surfaces based on candle soot[10] to form polymer microparticles has been demonstrated recently[12]. Our strategy to utilize superamphiphobic surfaces as „reactors" to fabricate monodisperse mesoporous supraparticles by evaporating nanoparticle dispersions takes advantage of the extreme liquid repellency of the superamphiphobic surfaces. The almost spherical shape of the droplets and the resulting low adhesion of the particles to the layer allow mesoporous supraparticles to be formed after evaporation. This new approach for

particle synthesis facilitates producing various sizes, compositions, and architectures of supraparticles by simple alternations with no consuming chemicals and energy.

The schematic illustration in **Figure 1**a shows the formation of the mesoporous supraparticle on the superamphiphobic surface from the nanoparticle (NP) aqueous dispersion drop. The NP dispersion drop on the superamphiphobic surface retains its spherical shape due to the high liquid repellency, leading to the supraparticle formation after evaporation. In order to realize this supraparticle synthesis concept, first, we prepared the superamphiphobic surface using the soot-templating method.[10] The highly porous silica structure based on the soot template was hydrophobized with 1H,1H,2H,2H-perfluorooctyltrichlorosilane to lower its surface energy (Figure 1b). Microscopic pockets of air are trapped in the porous silica structure beneath the liquid, is a key to superhydro- and superamphiphobicity; the liquid droplet sits on top of the protrusions while the interfacial tension of the liquid enforces a spherical shape of the droplet with a high receding contact angle of ≈163° for water. Contact angles were determined by laser scanning confocal microscopy (Figure1c), briefly called confocal microscopy, as the small contact area is not easily visible from the side. The high contact angle leads to the formation of nearly spherical drops of the NP dispersion.
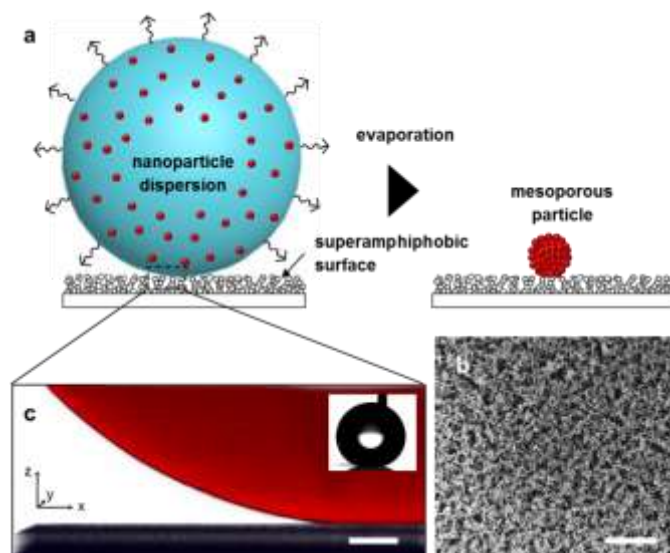

Figure 1. Drop of an aqueous nanoparticle dispersion on a soot-templated superamphiphobic surface. a) A schematic illustration of mesoporous supraparticle formation on the superamphiphobic surface. Due to the high liquid repellency, the shape of the evaporating drop remains spherical throughout the process. b) Scanning electron microscope (SEM) image of the highly porous structure of a superamphiphobic surface prepared by the soot deposition method[10] (scale bar: 10 μm). c) Interface between the drop and superamphiphobic surface imaged by confocal microscopy. Water (red) was fluorescently labeled with the Alexa488 dye for illustration. Reflection (gray) shows the porous superamphiphobic surface and the drop-air interface (scale bar: 50 μm). The inset is a side-view of the drop of the nanoparticle dispersion.

After dispensing 1 μL of an aqueous dispersion of TiO_2 NP (0.1 vol% of TiO_2 NP, diameter 21 nm, P25 Degussa Evonik) on the superamphiphobic surface, size and shape of the drop were monitored with a side-camera (**Figure 2**a). Throughout the evaporation process the

spherical shape was retained while the NP dispersion transformed into a solid particle. While the contact diameter decreased continuously, the contact angle θ stayed above 160˚ (Figure 2b). As predicted by theory[13],[14] for drops evaporating in constant contact angle mode, the volume $V^{2/3}$ of a sessile drop decreases linearly with time (Figure 2c). The nanoparticles hardly influence the evaporation rate, which was found to be $\frac{d(V^{2/3})}{dt} = (1108 \pm 10)$ μm²/s in the presence of nanoparticles and (980 ± 30) μm²/s for a sessile drops of pure water evaporating under the same conditions (θ = 160°, T = 22°C, relative humidity RH=42%). It indicates that the hydrophilic NPs remain inside the drop and do not affect the evaporation. For a detailed analysis see supporting information.

The evaporation kinetics indicates that the contact line of the drops slides freely over the superamphiphobic surface. This was verified by imaging evaporating drops of NP dispersion with confocal microscopy (Figure 2d). No contact line pinning was observed. Based on these results, we suggest the particle formation to proceed as illustrated in Figure 2e. The air-pockets at the interface lead to a low adhesion between the drop and the superamphiphobic surface. At the end of the evaporation, mesoporous supraparticles remained as spherical agglomerates of NPs. The final spherical supraparticle structure, measured by confocal microscopy in reflection mode (Figure 2f), revealed the small contact area with the superamphiphobic surface, which made detaching the particles easy. The mesoporous TiO_2 supraparticles do not require any purification as no organic auxiliaries where required during their synthesis. TiO_2 NPs are assembled by capillary force during drying. The maximal capillary pressure during drying for perfectly wetted particles of radius R is $\Delta P \approx 10\gamma/R$[15], where γ is the surface tension of the liquid. With $R = 12$ nm the pressure is of the order of 60 MPa. Such a pressure is sufficient to bring the particles in direct contact, where van der Waals forces add to the cohesion. Van der Waals forces are particularly strong between TiO_2 nanoparticles because of the high refractive index of 2.5 ~ 2.6, depending on its structure[16]. Therefore, the mesoporous supraparticles were highly stable and did not re-disperse to NPs in solvent for more than few months, if there were no strong external mechanical stress, e.g. ultra-sonication, allowing their application both, as powder and in dispersion.
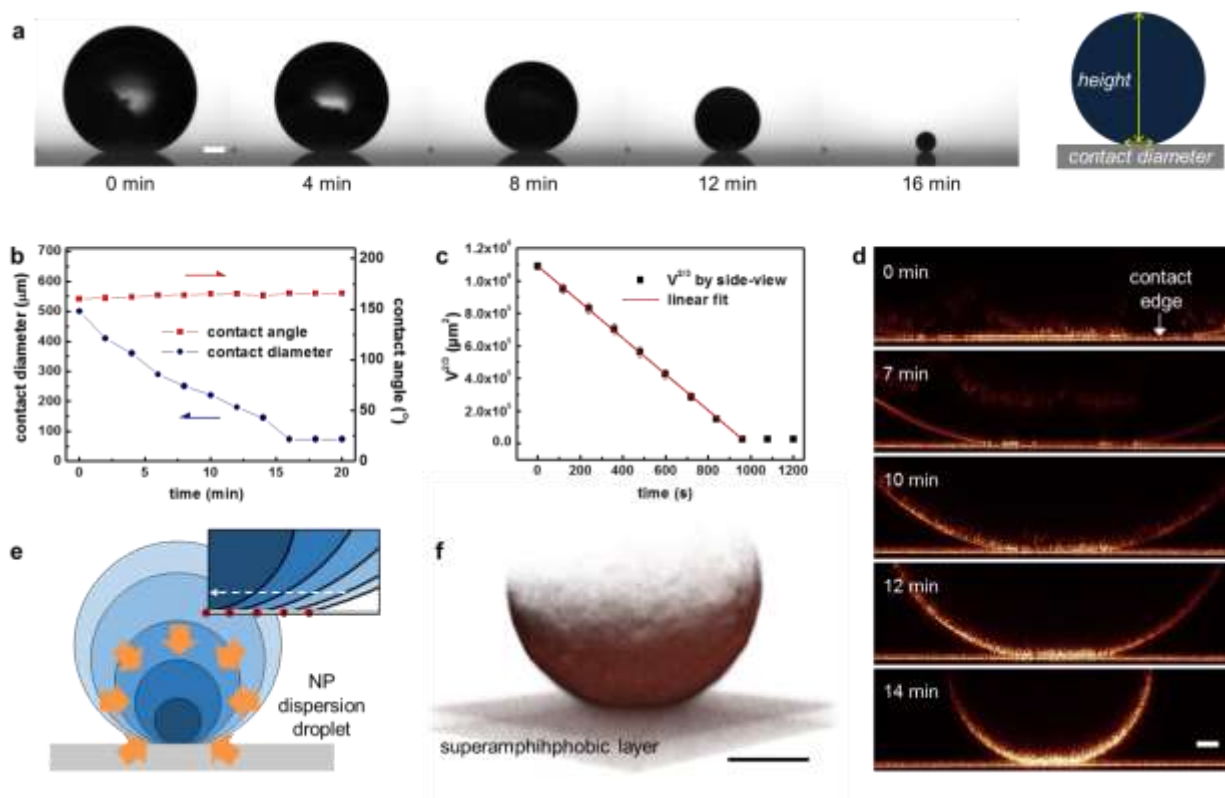
Figure 2. Supraparticle formation on a superamphiphobic surface. a) Side-view pictures of NP dispersion drop (initial volume: 1 µL) on the superamphiphobic surface at 22 °C and 42 ± 2 % RH (scale bar: 200 µm). The drop size decreased with time by evaporation, but the drop shape remained spherical. b) Contact diameter and contact angle variations of the evaporating drop estimated from side-view pictures in a). c) As expected for drops evaporating in constant contact angle mode, $V^{2/3}$ varies linearly with time. The volume was estimated from the height of the drop from the side-view picture in a) assuming that drop was otherwise completely spherical. d) NP dispersion drop on a superamphiphobic surface during water evaporation imaged by confocal microscopy (vertical cross-section, scale bar: 20 µm). e) A schematic illustration of the evaporation of the NP dispersion drop with moving contact line, forming the supraparticle. f) 3D image of a mesoporous TiO_2 supraparticle on the superamphiphobic surface imaged by confocal microscopy in reflection mode (scale bar: 50 µm).

We compared particle formation on the superamphiphobic surface with that on a flat hydrophobic glass surface (water advancing CA 125°, receding CA 93°) and a structured superhydrophobic surface (water advancing CA 156°, receding CA 115°). The superhydrophobic surface with a ~ 15 nm nano-roughness repels water, but not oils[17]. In contrast to superamphiphobic surfaces, on the flat hydrophobic surface the contact line of the drop was pinned on the substrate and the contact angle decreased during evaporation. Therefore, after evaporation, the surface film structure with cracks was formed since the volume was shrunken with the pinned contact line (Figure S3). On the superhydrophobic surface, the contact line of the NP dispersion drop slowly moved towards the center of the contact area. Its speed was, however, not as fast as the decreasing rate of the height, which leads to the formation of a cracked hemispherical shell structure (Figure S3). Therefore, the strong liquid repellency of superamphiphobic surfaces is essential for the contact line to slide

freely at constant and high apparent receding contact angle. This free sliding of the contact line is a prerequisite for the formation of spherical supraparticles.

The size of the mesoporous supraparticles could be controlled (**Figure 3**a) by adjusting the initial volume and concentration of the NP dispersion placed on the superamphiphobic surface. Supraparticles with diameters ranging from a few microns to sub-millimeter could be obtained by varying the initial concentration of the TiO_2 NPs (0.01 ~ 1 vol%) and the volume of the drops (0.3 ~ 4 μl). The porosity was 53 ± 1 %, as calculated from a comparison of the final particle size and the initial volume of the drop considering the NP concentration. The surface area of 53 m^2/g and the average pore size of 56 nm were characterized by Brunauer–Emmett–Teller (BET) analysis. Suspensions of hard, repulsive spheres are liquid-like at low concentration. As the volume fraction of the particles φ increases the suspension undergoes a transition to a disordered solid. This transition occurs at a critical volume fraction of 0.58[18]. In our case the volume fraction is on φ = 0.47, indicating that the NPs interact attractively, at least at short separation in the solution prior to drying of water[19].

In addition, mesoporous supraparticles of various metal oxides could be made. As an example, we fabricated spherical mesoporous TiO_2 and SnO_2 particles (Figure 3 b,c). The great flexibility of the process to vary materials and particle sizes also allowed the synthesis of heterogeneous supraparticles from two or even more components. We could, for example, fabricate multicomponent TiO_2/SnO_2, TiO_2/ZnO, and TiO_2/Fe_2O_3@SiO_2 particles (Figure 3d and Figure S5). The SnO_2, ZnO, and Fe_2O_3/SiO_2 core-shell (Fe_2O_3@SiO_2) NPs were prepared by chemical reduction process with diameters of (5 ± 0.5) nm, (6 ± 1.5) nm, and (11 ± 0.5) nm core with (6.5 ± 0.5) nm shell, respectively (Figure S4). The composite supraparticles can include two or more functions/functionalities, e.g. magnetism or more efficient catalytic activity by engineering their composition or band gap[6, 20]. Moreover, an inorganic/organic (TiO_2/polydopaminacrylamide) dispersion mixture was applied to demonstrate the formation of TiO_2/polydopaminacrylamide composite particles (Figure S5). TiO_2/polydopaminacrylamide forms a material with a high yield stiffness and hardness due to strong interfacial bonding through metal complexation by the dopamine surface ligand[21]. Not only mixed composite particles but also core-shell supraparticles could be formed *via* a sequential drying process with SnO_2 and TiO_2 NP dispersions. The SnO_2 core was made by evaporating a SnO_2 NP dispersion, followed by adding a TiO_2 NP dispersion to obtain the TiO_2 shell (Figure 3e).
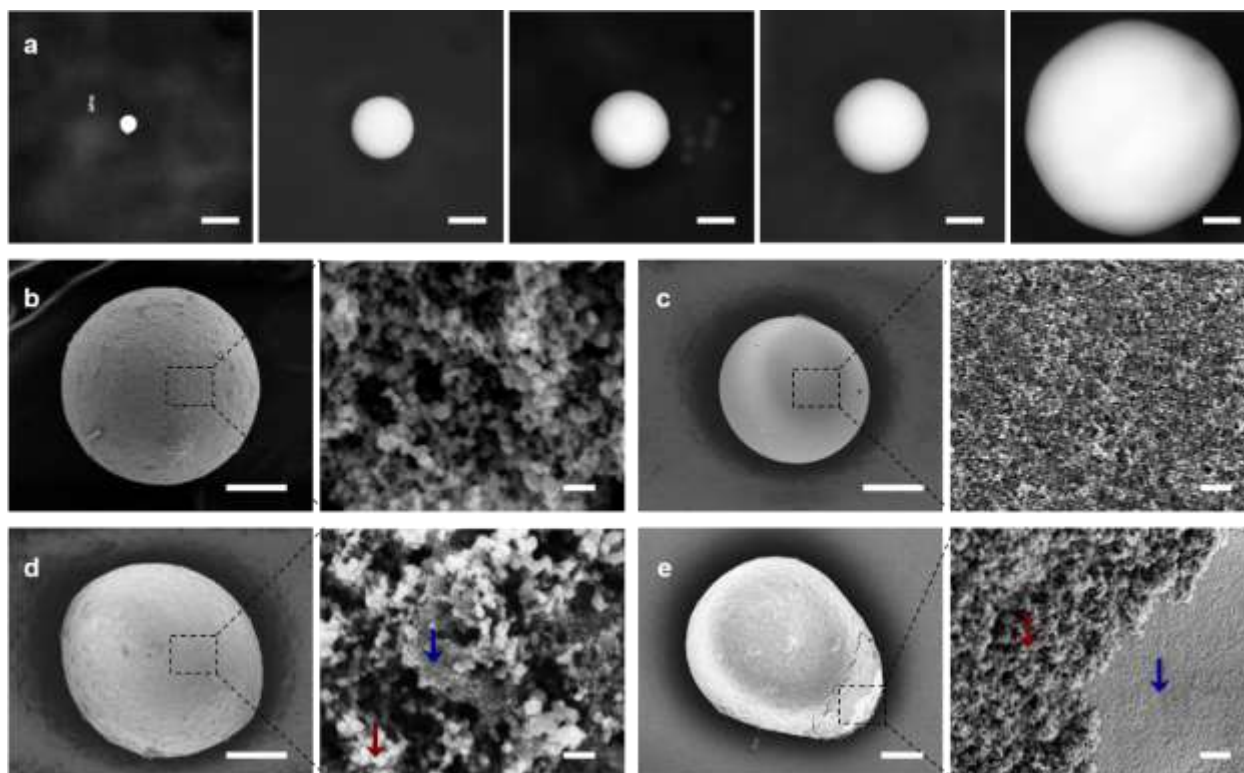
Figure 3. Mesoporous supraparticles with different sizes and materials. a) Optical microscope images of mesoporous TiO_2 supraparticles with different diameters (50 μm, 160 μm, 200 μm, 250 μm, and 550 μm). The particle size was controlled by changing the initial volume of the drop and the concentration of the NPs (from left to right: 0.01vol%-0.3 μL, 0.1 vol%-1 μL, 0.1vol%-2 μL, 0.1 vol%-4 μL, and 1vol%-4 μL of initial volume and concentration were used, respectively). The scale bars indicate 100 μm. b) - e) Mesoporous particles with different materials imaged by SEM. The scale bars in all images on the left are 50 μm, and magnified images on the right are 100 nm (except the right image of e) which is 1 μm). The mesoporous b) TiO_2 and c) SnO_2 particles were fabricated on the superamphiphobic surface from TiO_2 and SnO_2 NP aqueous dispersions, respectively. The TiO_2/SnO_2 heterogeneous particle d) was made from TiO_2/SnO_2 (0.07-0.03 vol%) mixture of NP dispersions. The $SnO_2@TiO_2$ core-shell particle e) was fabricated by a sequential evaporation with SnO_2 and TiO_2 dispersions. The blue and red arrows indicate SnO_2 and TiO_2, respectively.

Mesoporous semiconductor particles with variable sizes can be applied in a variety of research areas, e.g. as photocatalyst, for energy storage, or in solar cell devices. It also facilitates fabrication of tubular photocatalytic reactors for continuous reactions. In order to establish such a continuous tubular reactor, TiO_2 supraparticles were produced with homogeneous size introducing the catalytical activity of TiO_2. In fact, the soot-templated superamphiphobic surface was not completely stable for particle formation. It was shown that 20 ~ 50 nm of top layer of superamphiphobic surface was occasionally damaged by particle formation. But ~ 0.3 g of particles could be produced with homogeneous size (**Figure 4**a), and the surface was still superamphiphobic after production. The TiO_2 supraparticles were filled in a tubular reactor with 0.8 mm diameter polytetrafluoroethylene tube between two stainless filters with 2 μm pores as a dry phase powder (Figure 4b). The supraparticles with their large surface area are easier to fill in the tubular reactor than the NP powder directly.

6

Furthermore, since NPs pass through the filter or block the pores of filter, it is difficult to make a continuous reactor with classical NPs. Not only TiO_2 but also SnO_2, ZnO, and heterogeneous supraparticles synthesized on the superamphiphobic surface can be applied for different photocatalytic process. The photocatalytic activity of the TiO_2 supraparticles was demonstrated by bleaching a Rhodamine B solution passing through the reactor under UV illumination (UV source: LQ-400, Dr. Gröbel UV-Elektronik GmbH). The intensity was measured with a silicon photodiode sensor (Newport Co., model 818-sl/db) and was about 10 mW/cm^2.

A major disadvantage of the evaporation technique on superamphiphobic surfaces is the relatively long evaporation time as each particle is formed by evaporation from a single drop of the dispersion drop. In order to produce many particles in a short time, it was necessary to increase the drop dispensing frequency and to dispense smaller drops. A multi-nanodroplet-dispenser (Nano-Plotter, Gesim, Germany) was employed for fast and automatic particle production. The Nano-Plotter with a piezoelectric nano-tip (Figure 4c) dispensed droplets of reproducible volume with 1 kHz maximum dosing frequency. Such small droplets (~ 0.7 nL) of aqueous TiO_2 NP dispersions completely dry within few seconds and monodisperse mesoporous TiO_2 particles (diameter ~ 10 μm) were successfully formed on the superamphiphobic surface (Figure 4d,e). However these experiments also showed a limit with respect to particle size. When the drop size falls below a certain value, the decreasing rate of the height was faster than the movement of contact line, and the top of droplet collapsed during the last stage of evaporation. This collapse was previously found in the suprastructures formed on hydrophobic surfaces with pinned liquid contact line[7, 22]. However, even on superamphiphobic surfaces, the collapsed doughnut-like supraparticles were formed (Figure 4f) from small droplets (< 1 nL) due to its relatively fast evaporation by high surface-to-volume ratio.

Because of the small average spacing between protrusions of the soot-templated superamphiphobic surface, liquid repellency is guaranteed even for 10 μm-sized droplets. Whereas such small mesoporous microparticles could not form on e.g. superhydrophobic hierarchical micropillars[17] or superamphiphobic etched aluminum surfaces[23] (Figure S6), despite of the fact that large water droplets showed high contact angles (> 155˚ apparent static contact angle). Due to the large spacing between neighboring protrusions (> 10 μm) on these structures, NP dispersion droplet with a volumes $\lesssim$ ~ 1 nL were pinned between pillars or etched microstructures as the volume of droplet decreased by evaporation. The size limit is expected to be about one order of magnitude larger than the average distance between the asperities of the structured surface. Because the spacing in the overhang structures of the soot layer was 1 ~ 2 μm, particles with a radius < 5 μm could not be formed.

Another limitation in size arises from the difficulty in collecting the particles. Particles with diameters > 30 μm roll off the superamphiphobic surface and can be collected easily. Even though spherical particles with diameters of 10 ~ 30 μm were synthesized, they adhered to their initial position after water evaporation. Therefore, we exploited the self-cleaning properties of the superamphiphobic surface to collect small supraparticles using rolling water/ethanol mixture drops (Figure 4c). The particle collection by droplets was facilitated by the fact that the NPs did not re-disperse once they had been dried (Figure 4f,g).
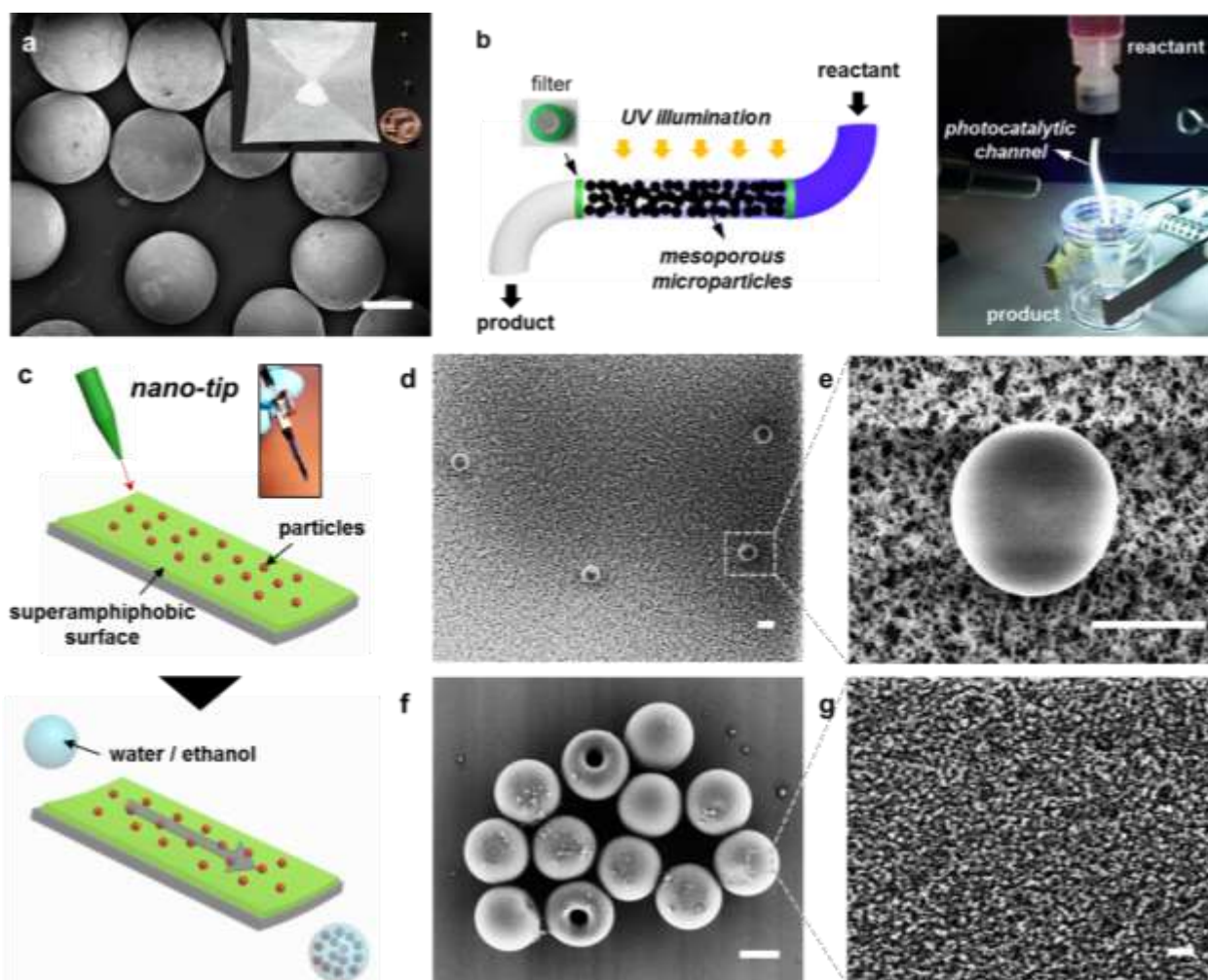
Figure 4. a) TiO$_2$ mesoporous supraparticles were produced from TiO$_2$ nanoparticle dispersions (0.1 vol%) dispensed by a fine micropipette (10 μL) and imaged by SEM. The inset shows produced particles as powder. b) A schematic illustration and picture of a tubular photocatalytic reactor for a continuous reaction. The tubular reactor was fabricated with mesoporous TiO$_2$ supraparticles filled in a 0.8 mm diameter polytetrafluoroethylene tube with 2 μm pore stainless filters. Rodamine B dye in water was decomposed continuously on the mesoporous TiO$_2$ particles under UV irradiation. c) A schematic illustration of the multiple particle production process on the superamphiphobic surface with a multi-nanodroplet-dispenser (Nano-Plotter). d), e) The mesoporous TiO$_2$ particles on the superamphiphobic surface were characterized by SEM. The TiO$_2$ NP (diameter 7 ± 2 nm) dispersion droplets were dispensed with a Nano-Plotter and transformed to mesoporous particles after water evaporation in few seconds. f), g) The mesoporous particles were collected by a water/ethanol (1:1 weight) mixture solution and characterized by SEM. The scale bars are 200 μm in a), 10 μm in d) - f) and 100 nm in g).

In conclusion, we demonstrated a generalized solvent-free fabrication process for mesoporous supraparticles from NP dispersions on superamphiphobic surface. As a result of the strong liquid repellence of the superamphiphobic surface, NP dispersion drops do not pin at the surface during evaporation but the contact line recedes easily. This leads to the formation of spherical mesoporous supraparticles, and the particles can be removed easily

from the superamphiphobic surfaces. Avoiding solvents prevents the contamination of a continuous phase by side products and organic auxiliaries such as templating surfactants, or stabilizers, starting compounds etc. Also a time-consuming or costly purification of the continuous aqueous phase is not required. Particle size, composition and architecture (e.g. heterogeneous particle and core/shell particle) can be varied by choosing the drop volume, concentration, type of NP, and sequence of deposition and evaporation steps. This flexibility in the synthetic process facilitates applying particles in numerous research areas with various materials, sizes, and functionalities. Moreover, the combination with a multi-nanodroplet-dispensing machine opens the door for fast, simple, low-cost fabrication of mesoporous supraparticles.

Experimental Section

Fabrication of the Superamphiphobic Surface and Supraparticle Formation Setup: As a template, soot particles were deposited on the substrate by candle soot deposition method[19]. Then 10 ~ 20 nm SiO_2 shell was coated on the deposited soot particles by chemical vapor deposition (CVD) of tetraethoxysilane (TES) catalyzed with ammonia. The soot was burned away at 550 ℃ realizing a fractal-like structure of SiO_2 with overhangs. The superamphiphobic surface was finally generated after surface modification with trichloro(1H,1H,2H,2H-perfluorooctyl)silane which induced lower surface energy. A multiple droplet dispensing system was constructed by employing a multi-nanodroplet dispensing machine (Nano-Plotter, maximum frequency: 1000 Hz) with piezoelectric nano-tip (GeSiM mbH, Germany).

Characterization of Mesoporous Supraparticles Fabrication Process: Mesoporous supraparticle formation by drying process was characterized by side camera (IDS uEye camera), optical microscope (Carl Zeiss Axiotech Vario 100HD), and laser scanning confocal microscope (confocal microscopy, Leica Microsystems TCS SP8). In order to investigate the interface between droplet and surface with confocal microscopy, transparent superamphiphobic surface was prepared on the microscope cover glass (Carl Roth GmbH, thickness: 170 ± 5 µm). In most cases the confocal microscopy operated in reflection mode, with a dry objective 40×/0.85 and excitation beam of a HeNe laser at 633 nm. In addition, size, structure and composition of produced mesoporous supraparticles were investigated with confocal microscopy and scanning electron microscope (SEM, 1530Gemini LEO=Zeiss).

Supporting Information
Supporting Information is available from the Wiley Online Library or from the author.

References

[1] a) H. X. Li, Z. F. Bian, J. Zhu, D. Q. Zhang, G. S. Li, Y. N. Huo, H. Li, Y. F. Lu, *J. Am. Chem. Soc.* **2007**, *129*, 8406; b) R. Y. Zhang, A. A. Elzatahry, S. S. Al-Deyab, D. Y. Zhao, *Nano Today* **2012**, *7*, 344.

[2] H. H. P. Yiu, H. J. Niu, E. Biermans, G. van Tendeloo, M. J. Rosseinsky, *Adv. Func. Mater.* **2010**, *20*, 1599.

[3] a) H. J. Koo, Y. J. Kim, Y. H. Lee, W. I. Lee, K. Kim, N. G. Park, *Adv. Mater.* **2008**, *20*, 195; b) M. A. Hossain, G. W. Yang, M. Parameswaran, J. R. Jennings, Q. Wang, *J. Phy. Chem. C* **2010**, *114*, 21878.

[4] a) X. L. Li, M. Gu, S. Y. Hu, R. Kennard, P. F. Yan, X. L. Chen, C. M. Wang, M. J. Sailor, J. G. Zhang, J. Liu, *Nat. Comm.* **2014**, *5*, 4105; b) S. J. Ding, J. S. Chen, Z. Y. Wang, Y. L. Cheah, S. Madhavi, X. A. Hu, X. W. Lou, *J. Mater. Chem.* **2011**, *21*, 1677.

[5] a) F. Lu, W. P. Cai, Y. G. Zhang, *Adv. Funct. Mater.* **2008**, *18*, 1047; b) H. Jiang, J. Q. Hu, F. Gu, C. Z. Li, *J. Phys. Chem. C* **2008**, *112*, 12138.

[6] S. H. Ahn, D. J. Kim, W. S. Chi, J. H. Kim, *Adv. Func. Mater.* **2014**, *24*, 5037.

[7] O. D. Velev, A. M. Lenhoff, E. W. Kaler, *Science* **2000**, *287*, 2240.

[8] a) J. R. Millman, K. H. Bhatt, B. G. Prevo, O. D. Velev, *Nat. Mater.* **2005**, *4*, 98; b) O. D. Velev, S. Gupta, *Adv. Mater.* **2009**, *21*, 1897; c) Y. S. Xia, Z. Y. Tang, *Chem. Comm.* **2012**, *48*, 6320; d) J. Il Park, T. D. Nguyen, G. D. Silveira, J. H. Bahng, S. Srivastava, G. P. Zhao, K. Sun, P. J. Zhang, S. C. Glotzer, N. A. Kotov, *Nat. Comm.* **2014**, *5*, 3593; e) B. de Nijs, S. Dussi, F. Smallenburg, J. D. Meeldijk, D. J. Groenendijk, L. Filion, A. Imhof, A. van Blaaderen, M. Dijkstra, *Nat. Mater.* **2015**, *14*, 56.

[9] a) V. Rastogi, S. Melle, O. G. Calderon, A. A. Garcia, M. Marquez, O. D. Velev, *Adv. Mater.* **2008**, *20*, 4263; b) M. Sperling, O. D. Velev, M. Gradzielski, *Angew. Chem. Int. Ed.* **2014**, *53*, 586; c) D. W. Lee, M. H. Jin, C. B. Lee, D. Oh, S. K. Ryi, J. S. Park, J. S. Bae, Y. J. Lee, S. J. Park, Y. C. Choi, *Nanoscale* **2014**, *6*, 3483; d) A. G. Marin, H. Gelderblom, A. Susarrey-Arce, A. van Houselt, L. Lefferts, J. G. E. Gardeniers, D. Lohse, J. H. Snoeijer, *Proc. Natl. Acad. Sci. USA* **2012**, *109*, 16455.

[10] X. Deng, L. Mammen, H. J. Butt, D. Vollmer, *Science* **2012**, *335*, 67.

[11] Z. L. Chu, S. Seeger, *Chem. Soc. Rev.* **2014**, *43*, 2784.

[12] X. Deng, M. Paven, P. Papadopoulos, M. Ye, S. Wu, T. Schuster, M. Klapper, D. Vollmer, H. J. Butt, *Angew. Chem. Int. Ed.* **2013**, *52*, 11286.

[13] R. G. Picknett, R. Bexon, *J. Col. & Interf. Sci.* **1977**, *61*, 336.

[14] C. J. Liu, E. Bonaccurso, H. J. Butt, *Phys. Chem. Chem. Phys.* **2008**, *10*, 7150.

[15] W. A. Henson, D. A. Taber, E. B. Bradford, *Indust. & Engineer. Chem.* **1953**, *45*, 735; J. L. Hilden, K. P. Trumble, *J. Colloid Interface Sci.* **2003**, *15*, 463.

[16] F. L. Leite, C. C. Bueno, A. L. Da Roz, E. C. Ziemath, O. N. Oliveira, *Int. J. Mol. Sci.* **2012**, *13*, 12773.

[17] S. Wooh, J. H. Koh, S. Lee, H. Yoon, K. Char, *Adv. Funct. Mater.* **2014**, *24*, 5550.

[18] P. N. Pusey, W. v. Megen, *Phy. Rev. Lett.* **1987**, *59*, 2083.

[19] P. N. Segre, V. Prasad, A. B. Schofield, D. A. Weitz, *Phy. Rev. Lett.* **2001**, *86*, 6042.

[20] C. Cheng, A. Amini, C. Zhu, Z. L. Xu, H. S. Song, N. Wang, *Sci. Rep.* **2014**, *4*, 4181.

[21] F. Liaqat, M. N. Tahir, E. Schechtel, M. Kappl, G. K. Auernhammer, K. Char, R. Zentel, H.-J. Butt, W. Tremel, *Macromol. Rapid Commun.* **2015**, *36*, 1129.

[22] V. Rastogi, A. A. Garcia, M. Marquez, O. D. Velev, *Macromol. Rapid Commun.* **2010**, *31*, 190.

[23] S. Peng, X. J. Yang, D. Tian, W. L. Deng, *ACS Appl. Mater. Interf.* **2014**, *6*, 15188.

The Table of Contents
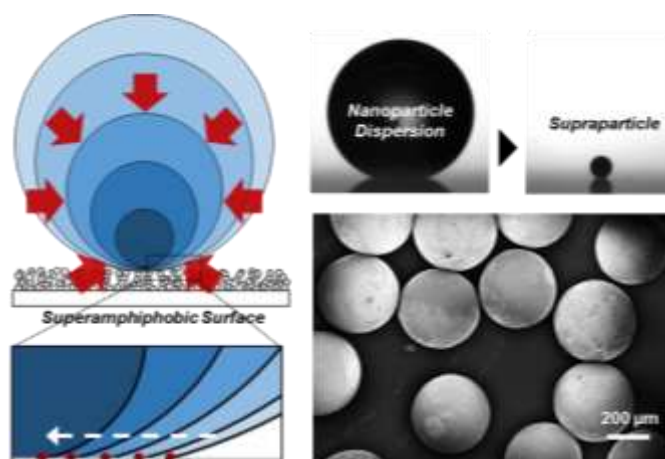
A method for mesoporous supraparticle synthesis on superamphiphobic surfaces is designed. Therefore, supraparticles assembled with nanoparticles are synthesized by evaporation of nanoparticle dispersion drops on the superamphiphobic surface. For synthesis, no further purification is required and no organic solvents are wasted. Moreover by changing the conditions such as drop size and concentration, supraparticles of different size, composition, and architecture are fabricated.

Keywords: superamphiphobic surface, supraparticle, wetting, drop evaporation, mesoporous particle